

# Understanding Channel Access in Timely Status Updates: Random Access or Scheduled Access?

Zhiling Yue<sup>\*†</sup>, Yuting Tang<sup>\*†</sup>, Nikolaos Pappas<sup>‡</sup>, Yaru Fu<sup>§</sup>, and Howard H. Yang<sup>\*†</sup>

<sup>\*</sup>Zhejiang University/University of Illinois Institute, Zhejiang University, Haining, China

<sup>†</sup>National Mobile Communications Research Laboratory, Southeast University, Nanjing, China

<sup>‡</sup>Dept. of Computer and Information Science, Linköping University, Linköping, Sweden

<sup>§</sup>School of Science and Technology, Hong Kong Metropolitan University, Hong Kong

**Abstract**—We investigate the role of channel access schemes in enhancing the timeliness of status updates in sensor networks. Specifically, we model the large-scale sensor network as a Poisson cellular network and derive the network average Age of Information (AoI) under two channel access schemes: random and scheduled access. Our findings reveal that the effectiveness of these schemes is influenced by the signal-to-interference ratio (SIR) decoding threshold, which often reflects the length of communication data. For short-packet communications, performance differences among various channel access strategies are minimal, and the gains from scheduling are limited; in fact, some simple scheduling strategies may not outperform basic random strategies. Conversely, scheduled access schemes demonstrate a distinct performance advantage for long-packet communications. The round robin scheme consistently yields the best performance among the four protocols we examined—slotted ALOHA, frame slotted ALOHA, random scheduling, and round robin scheduling. This is due to its ability to mitigate intra-cell interference and regularize both status updates and channel access periods for each sensor, which is particularly beneficial in reducing AoI.

## I. INTRODUCTION

Acquiring timely status information is essential for decision-making in many Internet of Things (IoT) applications [1]. To quantify timeliness, the Age of Information (AoI) has been proposed as a key metric [2] and has received considerable attention. Unlike traditional metrics such as delay and throughput, AoI is measured from the destination’s perspective and quantifies the time elapsed since the state information was last generated [3].

In wireless IoT networks, multiple sensors usually share a limited spectrum to enable connectivity. The efficient allocation of these scarce wireless resources to facilitate the timeliness of information delivery has become a critical challenge. Efficient channel access strategies are essential for addressing

The work of Z. Yue, Y. Tang, and H. H. Yang are supported in part by the National Key R&D Program of China under Grant 2024YFE0200700, in part by the open research fund of National Mobile Communications Research Laboratory, and in part by the National Natural Science Foundation of China under Grant 62201504. The work of Z. Yue has been supported by Zhejiang University. The work of Y. Fu was supported in part by the Hong Kong Research Matching Grant (RMG) in the Central Pot under Project No. CP/2022/2.1, and in part by the Team-based Research Fund under Project No. TBRF/2024/1.10 The work of N. Pappas has been supported in part by the Swedish Research Council (VR), Excellence Center at Linköping – Lund in Information Technology (ELLIIT), and the European Union (ETHER, 101096526 and 6G-LEADER, 101192080). (Corresponding Author: Howard H. Yang.)

this issue. Early works focused on analyzing the AoI based on traditional slotted ALOHA (SA) protocols, aiming to assess its performance in the context of real-time data transmission [4]. However, the SA scheme is designed primarily to optimize conventional metrics such as throughput, focusing on reducing channel contention to improve transmission success probability. Therefore, it does not perform well in terms of AoI performance. Noticing this limitation, [5] introduced an age threshold and proposed a new update strategy called Threshold ALOHA. [6] introduced an index to denote the urgency of updates for each source and spectral resources allocated based on the urgency index.

These studies primarily focused on single-cell scenarios, where multiple source nodes update information to a common receiver. However, practical wireless network systems usually consist of multiple cells. Due to the broadcast nature of the wireless medium, simultaneous transmissions from different sources can interfere with each other, thereby degrading the communication quality. In this case, adopting a signal-to-interference-plus-noise ratio (SINR) or signal-to-interference ratio (SIR) model, combined with stochastic geometry tools, is more suitable for analysis, as it incorporates these essential elements, providing a more accurate representation of network performance. In [7], [8], the authors built upon the SA scheme and jointly applied stochastic geometry and queuing theory to decouple the spatiotemporal entanglement of nodes to perform AoI analysis in wireless networks. Given the shortcomings of the SA scheme, [9] analyzed AoI performance under a modified channel access scheme termed Age-Threshold Slotted ALOHA (TSA). Additionally, [10] introduced a further variation, frame-slotted ALOHA (FSA), demonstrating that incorporating a frame structure into the SA protocol can significantly improve network AoI performance. These distributed random access protocols are advantageous for low-cost devices with limited communication resources.

However, in above schemes, the decision to transmit is entirely made by individual nodes without centralized coordination. Lack of planning inevitably leads to transmission collisions, which degrade AoI performance. In contrast, scheduled access protocols can regularize transmissions within each cell, reducing interference and improving communication quality. For instance, [4] analyzed the AoI performance under a feedback-based scheduled access scheme, demonstrating that

## II. SYSTEM MODEL

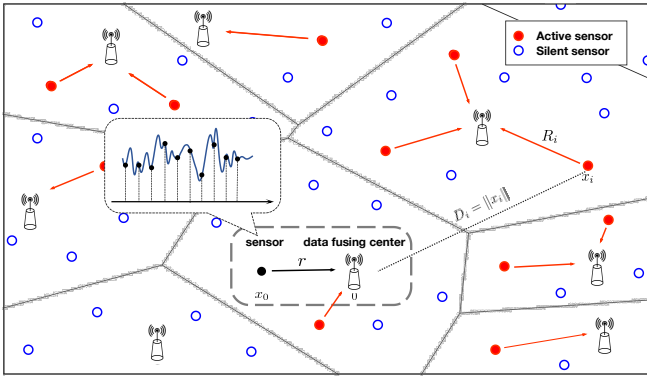


Fig. 1. A snapshot of the wireless network under consideration, where circles represent sensors that update status information to their designated data-fusing centers. The black circle represents the typical sensor, red circles denote other active sensors, and blue circles indicate inactive sensors.

the Round Robin (RR) approach outperforms the distributed SA scheme. [11] introduced four AoI-oriented scheduling protocols—Greedy, Randomized, Max-Weight, and Whittle’s Index policies—and analyzed their respective performances. These scheduling approaches are primarily designed for single-cell scenarios. The impact of scheduling strategies on AoI performance in large-scale networks remains unclear. Moreover, while scheduled access schemes can offer performance advantages over random access methods, the gains come at the cost of increased overhead and higher complexity. When such trade-offs are justified remains an open question.

In this paper, we develop an analytical framework to examine AoI performance across different channel access strategies in large-scale wireless networks, considering a realistic model of IoT sensor networks. Through mathematical analysis and numerical results, we provide a detailed assessment of the gains achievable through the additional signaling costs incurred by scheduled access for AoI improvement. Our main contributions are summarized below.

- We develop a mathematical framework to characterize network AoI performance across different channel access schemes, encompassing essential features of a wireless system, such as update rate, channel fading, path loss, and interference.
- We derive analytical expressions for the network average AoI under four channel access protocols: SA, FSA, random scheduling (RS), and RR. Based on the analysis, we conduct a comparative investigation of the four protocols and their impact on network AoI performance.
- Our simulation results validate the accuracy of the analysis, revealing that the additional costs associated with scheduled access schemes do not always yield the expected gains; in fact, significant improvements in AoI performance under scheduled access are observed only when the threshold is relatively high.

### A. Network Structure

We consider the wireless network illustrated in Fig. 1, which consists of multiple sensors and DFCs deployed on the Euclidean plane. The DFCs are distributed according to a homogeneous Poisson point process (PPP)  $\Phi_d$  with spatial density  $\lambda$ . Within the coverage area of each DFC—represented by a Voronoi cell generated from  $\Phi_d$ — $K$  sensors are uniformly distributed in space, with their locations denoted by  $\Phi_s$ .

In this network, each sensor aims to transmit a sequence of information packets containing its most recent updates to its designated DFC over time. We assume that every sensor transmits at a fixed power  $P_{tx}$ , using a shared spectrum. Communication is subject to small-scale fading, modeled by a Rayleigh distribution with unit mean, and large-scale path loss following power-law attenuation. We also assume that channel fading varies independently over time and space [12].

### B. Transmission Protocols

We consider a discrete-time system in which time is divided into equal-length slots, each long enough to accommodate a single packet transmission. We assume the network is synchronized. At the beginning of each time slot, sensors decide whether to perform a status update. If a sensor decides to update, it packages the sample data into an information packet and transmits it to the DFC.

We assume that data packets are uniform in size, and each requires a single time slot for transmission. A transmission is successful if the signal-to-interference ratio (SIR) at the destination exceeds a decoding threshold  $\theta$ ; otherwise, the transmission fails. Since the time scale of fading and packet transmission is much shorter than that of spatial dynamics, we consider a static network topology; specifically, an arbitrary but fixed point pattern is established at the start and remains unchanged throughout all subsequent time slots.

We investigate the effect of two channel access schemes, random access and scheduled access, on timely status updates.

1) *Random Access*: There is no centralized scheduler, hence channel access decisions are designated to the sensors. We will investigate two representative random access protocols, as detailed below.

- *Slotted ALOHA (SA)*: At the beginning of any given time slot, sensors activate independently with probability  $\eta_{SA}$  to collect data and transmit packets through the radio channel.
- *Frame Slotted ALOHA (FSA)*: A fixed number of consecutive time slots are encapsulated into a frame, where the framesize is denoted as  $F$ . At the beginning of each frame, sensors autonomously decide whether to generate new data during that frame with probability  $\eta_{FSA}$ . If a sensor decides to update, it randomly selects one time slot within the frame to transmit; otherwise, it remains silent throughout this frame period.

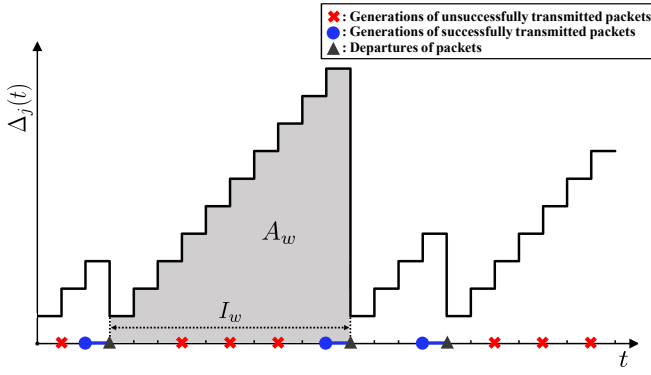


Fig. 2. An example of the evolution of the age of information  $\Delta_j(t)$ .

2) *Scheduled Access*: The DFCs serve as coordinators to schedule channel access for the sensors in their cells. We will examine two distinct scheduled access protocols, outlined as follows.

- *Random Scheduling (RS)*: At the beginning of each time slot, each DFC activates with probability  $\eta$ , and then selects one sensor in its coverage uniformly at random for status update.
- *Round Robin (RR)*: The sensors within each cell are indexed from 1 to  $K$ . At the onset of each time slot, the DFC activates a probability of  $\eta$  and sequentially selects one sensor to update the status information.

### C. Performance Metrics

As illustrated in Fig. 2, AoI measures the time elapsed since the last successfully delivered update package was generated from the source node. Formally, it is defined (on the transmitter-receiver pair  $j$ , denoted as link  $j$ ) as follows

$$\Delta_j(t) = t - G_j(t), \quad (1)$$

where  $G_j(t)$  is the generation time of the most recent packet successfully delivered to the receiver at the end of time slot  $t$ .

We use the network average AoI to evaluate the age performance. Concretely, the time-average AoI of link  $j$  is

$$\bar{\Delta}_j = \lim_{T \rightarrow \infty} \frac{1}{T} \sum_{t=1}^T \Delta_j(t). \quad (2)$$

Then, the network-wide average AoI [7], [13] is given by

$$\bar{\Delta} = \lim_{R \rightarrow \infty} \frac{\sum_{j: x_j \in B(0, R)} \bar{\Delta}_j}{\lambda \pi R^2}, \quad (3)$$

where  $x_j$  represents the location of sensor  $j$ ,  $B(0, R)$  represents a disk centered at the origin with a radius of  $R$ . By the stationarity and ergodicity of the point process, we have

$$\bar{\Delta} = \mathbb{E}[\bar{\Delta}_0]. \quad (4)$$

## III. ANALYSIS

### A. Preliminaries

According to Slivnyak-Mecke theory [14], we can focus on the performance of a *typical link*, which has the receiver, i.e.

DFC, situated at the origin. We index this link pair as 0. We consider an interference-limited scenario where thermal noise is negligible. Then, when the typical sensor updates at time slot  $t$ , the received SIR can be expressed as

$$\text{SIR}_{0,t} = \frac{P_{\text{tx}} h_{0,t} r^{-\alpha}}{\sum_{i \in \Phi_f} P_{\text{tx}} h_{i,t} v_{i,t} D_i^{-\alpha}}, \quad (5)$$

where as viewed from the perspective of this link,  $\Phi_f$  is the spatial distribution of potential interference sources with channel access permission,  $r = \|x_0\|$  denotes the distance between the typical sensor-DFC pair,  $\alpha$  is the path loss exponent,  $h_{i,t} \sim \exp(1)$  represents the channel fading from sensor  $i$  to the typical DFC and  $D_i = \|x_i\|$  is the corresponding distance, and  $v_{i,t} \in \{0, 1\}$  serves as an indicator of the active state of sensor  $i$  at time  $t$  where  $v_{i,t} = 1$  represents sensor  $i$  is active and accessing the channel, while  $v_{i,t} = 0$  otherwise. We assume the network has reached the stationary state, upon which the temporal dynamics of SIR over each link is independent and identically distributed (i.i.d.) over time. Hence, we can remove the time index  $t$  from the subscript in the following analysis.

Since the SIR is governed by various random variables, including channel fading, each sensor's active state and location, we use the *conditional transmission success probability* [15] to characterize its statistical behavior. Formally, conditioned on the spatial deployment  $\Phi \triangleq \Phi_s \cup \Phi_d$ , the conditional transmission success probability of the typical link is

$$\mu_0^\Phi = \mathbb{P}(\text{SIR}_0 > \theta \mid \Phi). \quad (6)$$

From the result in [16], the distance between the typical sensor-DFC pair is approximately distributed as a rescaled Rayleigh distribution with the probability density function

$$f_r(r) = 2a\pi\lambda r \exp(-a\pi\lambda r^2), \quad (7)$$

where  $a$  is the correlation term related to the network load conditions, and the condition  $a \geq 1$  always holds.

Notably, the channel access scheme affects the distribution of  $\mu_0^\Phi$ , which influences the network average AoI. As such, we quantify their effects in the following.

### B. Random Access

Under random access schemes, all sensors independently decide whether to become active or not. To equal the average update rate for each sensor under the random and scheduled access scenarios, we stipulate the updating protocol  $\eta_{\text{SA}} = \eta/K$  for SA and  $\{\eta_{\text{FSA}}, F\} = \{\eta, K\}$  for FSA.

Due to the correlation with the deployment of DFCs, the spatial distribution of sensors does not follow a PPP, posing challenges for the analysis. Fortunately, this dependence is generally weak and negligible [17]. Therefore, we approximate  $\Phi_s$  as a homogeneous PPP with intensity  $K\lambda$ .

Seen from the typical DFC, every other sensor could be a potential interferer in random access mode, making the effective interference domain expressible as  $\Phi_f^R = \Phi_s \setminus x_0$ . Subsequently, we can derive an preliminary expression for

(6) via a similar vein to that in [10]. The detailed result is presented in the following lemma.

**Lemma 1:** *Given point process  $\Phi$ , the conditional transmission success probability over the typical link under random access schemes is*

$$\mu_{0,R}^{\Phi} = \prod_{x_i \in \Phi_f^R} \left( 1 - \frac{\eta/K}{1 + \frac{\|x_i\|^\alpha}{\theta r^\alpha}} \right). \quad (8)$$

*Proof:* Please see Appendix A.  $\square$

Leveraging this intermediate result, we analyze the AoI performance under the SA and FSA protocols.

1) *Pure Slotted ALOHA:* Given the point process  $\Phi$ , the typical link collects a new update successfully in each time slot with probability  $\eta_{SA} \mu_{0,R}^{\Phi}$ . Consequently, AoI over the typical link can be regarded as following a geometric distribution with parameter  $\eta_{SA} \mu_{0,R}^{\Phi}$ , and we can calculate the conditional average AoI as follows

$$\bar{\Delta}_{0,SA}^{\Phi} = \frac{K}{\eta \mu_{0,R}^{\Phi}}. \quad (9)$$

To facilitate exposition in the sequel, we denote by  $\delta = 2/\alpha$  and  $C(\delta) = \Gamma(1-\delta)\Gamma(1+\delta)$ , where  $\Gamma(x) = \int_0^\infty t^{x-1} e^{-t} dt$  is the standard Gamma function [15]. Then, by taking an expectation of (9) on  $\Phi$ , we obtain the network average AoI under SA.

**Theorem 1:** *Under the SA protocol, if*

$$\frac{1}{a} \eta \theta^\delta C(\delta) \left( 1 - \frac{\eta}{K} \right)^{\delta-1} < 1, \quad (10)$$

*the network average AoI is*

$$\bar{\Delta}_{SA} = \frac{aK}{\eta \left( a - \frac{\eta \theta^\delta C(\delta)}{(1-\frac{\eta}{K})^{1-\delta}} \right)}; \quad (11)$$

*otherwise, the network average AoI is unbounded.*

*Proof:* Please see Appendix B.  $\square$

In practice, the path loss exponent  $\alpha$  usually satisfies  $\alpha > 2$ , hence  $0 < \delta < 1$ . Using Bernoulli's inequality, we have  $(1 - \frac{\eta}{K})^{1-\delta} \leq 1 - (1-\delta)\frac{\eta}{K}$ . As such, we can bound the (complement of) condition (10) as

$$\eta \geq \frac{aK}{K\theta^\delta C(\delta) + a(1-\delta)}, \quad (12)$$

in which  $\bar{\Delta}_{SA}$  will be infinite. Note that (12) is a sufficient condition rather than a necessary one.

By fixing the decoding threshold  $\theta = 0$ dB, if  $\alpha \rightarrow 2$ , the AoI is always unbounded regardless of the parameter pair  $(\eta, K)$  taking any values. Moreover, even as  $\alpha \rightarrow 4$ , the AoI will not converge for  $\eta$  values above approximately half of its domain (i.e.,  $\eta > 0.5$ ).

2) *Frame Slotted ALOHA:* Conditioned on the spatial deployment  $\Phi$ , we can derive the conditional AoI under FSA protocol over the typical link as [10]

$$\bar{\Delta}_{0,FSA}^{\Phi} = \frac{K^2-1}{12K} \eta \mu_{0,R}^{\Phi} + \frac{K}{\eta \mu_{0,R}^{\Phi}} + \frac{1-K}{2}. \quad (13)$$

Then, we can adopt a similar approach to average out  $\Phi$  and obtain the following result.

**Theorem 2:** *Under the FSA protocol, if the condition (10) holds, the network average AoI is*

$$\bar{\Delta}_{FSA} = \frac{K^2-1}{12K} \cdot \frac{a\eta}{a+\eta\theta^\delta C(\delta)} + \frac{aK}{a\eta - \frac{\eta^2\theta^\delta C(\delta)}{(1-\frac{\eta}{K})^{1-\delta}}} + \frac{1-K}{2}; \quad (14)$$

*otherwise, the network average AoI is unbounded.*

*Proof:* We omit the proof due to space limit.  $\square$

### C. Scheduled Access

In scheduled access schemes, DFCs act as schedulers to coordinate data updates among sensors. Under this mode, the link's active state is influenced by two factors: at the cell-level, the DFC is active with probability  $\eta$ ; at the sensor-level, it depends on whether the sensor is selected to access the radio channel.

Since the DFCs have the ability to manage the channel access permissions, ensuring that only one sensor in each cell is granted access at a time, the intra-cell interference can be effectively mitigated, while only the inter-cell interference remains. However, because of the correlation arising from the deployment of DFCs, the spatial distribution of interferers' positions no longer follows PPP, posing challenges for the analysis. In response, we adopt the approach in [18] to approximate the locations of interferers as a *non-homogeneous PPP*, which is detailed in the subsequent.

**Approximation 1:** *Under the scheduled access scheme, from the perspective of the typical DFC, the interfering nodes  $\Phi_f^S$  approximately constitute a non-homogeneous PPP with a distance-dependent intensity, given as*

$$\lambda(x) = \lambda \left( 1 - \exp \left( -\frac{12}{5} \pi \lambda \|x\|^2 \right) \right). \quad (15)$$

Moreover, according to the status update policy, we can treat each (potential) interfering node as independently activated with probability  $\eta$ . As such, we have the conditional transmission success probability as

$$\mu_{0,S}^{\Phi} = \prod_{x_i \in \Phi_f^S} \left( 1 - \frac{\eta}{1 + \frac{D_f^\alpha}{\theta r^\alpha}} \right), \quad (16)$$

where  $\Phi_f^S$  denotes the positions of the interferers.

In what follows, we use this model to analyze the network average AoI under two scheduled access protocols, namely, RS and RR, respectively.

1) *Random Scheduling:* By fixing the point process  $\Phi$ , we have an intermediate result for the network average AoI.

**Lemma 2:** *Conditioned on the spatial topology  $\Phi$ , the time-average AoI under RS over the typical link is*

$$\bar{\Delta}_{0,RS}^{\Phi} = \frac{K}{\eta \mu_{0,S}^{\Phi}}. \quad (17)$$

While the conditional average AoI expressions under RS and SA have the same form, the difference lies in the interference statistics. By deconditioning the above with respect to  $\Phi$ , we

can obtain the analytical expression for the network average AoI.

**Theorem 3:** *The network average AoI under the RS protocol is given by*

$$\bar{\Delta}_{\text{RS}} = \frac{aK}{\eta} \int_0^\infty \exp\left(-az + z \int_0^\infty \frac{\eta(1 - e^{-\frac{12}{5}zq})dq}{1 - \eta + \frac{q^{1/\delta}}{\theta}}\right) dz. \quad (18)$$

*Proof:* Please see Appendix C.  $\square$

2) *Round Robin:* In this approach, fixing spatial topology  $\Phi$ , the dynamics of status updates across each wireless link can be conceptualized as a round-based Bernoulli process. We denote the probability of activation and transmission success probability by  $\eta$  and  $\mu_{0,S}^\Phi$ , respectively. Utilizing a graphical method [10], we can derive the expression for the conditional AoI over the typical link.

**Lemma 3:** *Given the point process  $\Phi$ , the time-average AoI of the typical link under the RR protocol is*

$$\bar{\Delta}_{0,\text{RR}}^\Phi = \frac{K}{\eta\mu_{0,S}^\Phi} + \frac{1-K}{2}. \quad (19)$$

*Proof:* Please see Appendix D.  $\square$

Consequently, we can average out the randomness in  $\Phi$  and obtain the following.

**Theorem 4:** *The network average AoI under the RR access protocol is given by*

$$\bar{\Delta}_{\text{RR}} = \frac{aK}{\eta} \int_0^\infty \exp\left(-az + z \int_0^\infty \frac{\eta(1 - e^{-\frac{12}{5}zq})dq}{1 - \eta + \frac{q^{1/\delta}}{\theta}}\right) dz + \frac{1-K}{2}. \quad (20)$$

*Proof:* We follow the same derivation process as in Theorem 3, so it is omitted here.  $\square$

#### D. Discussions

Based on the theoretical results, we compare the AoI performance under different channel access schemes. We consider a normal network model where  $K > 2$ , with suitable values for  $\eta$  and  $\theta$ , to ensure that the AoI remains finite.

1) *General Case:* Firstly, we subtract the network average AoI performance under SA to that under FSA and arrive at the following

$$\begin{aligned} \bar{\Delta}_{\text{FSA}} - \bar{\Delta}_{\text{SA}} &= \frac{K^2-1}{12K} \times \frac{a\eta}{a+\eta\theta^\delta C(\delta)} - \frac{K-1}{2} \\ &\leq \frac{K^2-1}{12K} - \frac{K-1}{2} = -\frac{(5K-1)(K-1)}{12K} < 0. \end{aligned} \quad (21)$$

This result indicates that under the same update rate, FSA always produces a smaller network average AoI than SA, since it not only reduces the probability of simultaneous transmissions from nearby interfering sources, but also equalizes the update intervals of each source node.

Next, we conduct the same operation to the network average AoI under RS and RR and obtain the following

$$\bar{\Delta}_{\text{RR}} - \bar{\Delta}_{\text{RS}} = \frac{1-K}{2} < 0. \quad (22)$$

This result shows that when each DFC serves multiple users, the AoI performance under the RR scheme is always better than that under the RS scheme. It also indicates that imposing fairness in scheduling policy designs is instrumental in improving AoI performance.

**Remark 1:** *More regular update modes will optimize AoI performance in both random and scheduled access schemes.*

2) *Special Case:* The performance ranking among different strategies becomes uncertain as the decoding threshold varies. Here, we present a special case where  $\theta \rightarrow 0$ . This scenario is particularly relevant to short-packet communication, including applications such as wireless sensor networks, IoT devices, and real-time control systems.

In this case, we rewrite the AoI for SA according to (31) as follows

$$\begin{aligned} \bar{\Delta}_{\text{SA}} &= \frac{aK}{\eta} \int_0^\infty \exp\left(-az + z\eta \int_0^\infty \frac{1}{1 - \eta/K + q^{1/\delta}/\theta} dq\right) dz \\ &= \frac{aK}{\eta} \int_0^\infty \exp\left(-az + z\eta \left( \underbrace{\int_0^{C\theta^\delta} \frac{dq}{1 - \frac{\eta}{K} + \frac{q^{1/\delta}}{\theta}}}_{Q_1} + \underbrace{\int_{C\theta^\delta}^\infty \frac{dq}{1 - \frac{\eta}{K} + \frac{q^{1/\delta}}{\theta}}}_{Q_2} \right)\right) dz \\ &\stackrel{(a)}{\approx} \frac{aK}{\eta} \times \int_0^\infty \exp\left(-az + z\eta \int_{C\theta^\delta}^\infty \frac{1}{q^{1/\delta}/\theta} dq\right) dz \end{aligned} \quad (23)$$

where  $C \gg 1$  is a constant, and (a) follows because as  $\theta \rightarrow 0$ , we have  $Q_1 \rightarrow 0$ , while in  $Q_2$ ,  $\frac{q^{1/\delta}}{\theta} \geq C^{1/\delta} \gg 1$ , which leads to  $Q_2 \approx \int_{C\theta^\delta}^\infty \frac{dq}{q^{1/\delta}/\theta}$ . Similarly, we can approximate the network AoI under RS scheme as

$$\bar{\Delta}_{\text{RS}} \approx \frac{aK}{\eta} \times \int_0^\infty \exp\left(-az + z\eta \int_{C\theta^\delta}^\infty \frac{1 - e^{-\frac{12}{5}zq}}{q^{1/\delta}/\theta} dq\right) dz. \quad (24)$$

A comparison between (23) and (24) shows that RS scheme performs better than SA scheme in this scenario. However, this gain is not significant. As  $\theta \rightarrow 0$ , we observe the following from expressions (23) and (24)

$$\bar{\Delta}_{\text{SA}} \approx \bar{\Delta}_{\text{RS}} \approx \frac{aK}{\eta}. \quad (25)$$

From (21), we know that in this case, the gap between FSA and SA is approximately

$$\bar{\Delta}_{\text{FSA}} - \bar{\Delta}_{\text{SA}} \approx \frac{(K-1)(6K - \eta K - \eta)}{12K}. \quad (26)$$

This gap is almost solely related to the number of sensors covered by the DFCs, which increases with  $K$ . When we consider a general scenario where each DFC serves multiple sensors, this gap is noticeable.

Additionally, by comparing the network average AoI under FSA and RR in this scenario, we have

$$\begin{aligned} \bar{\Delta}_{\text{RR}} - \bar{\Delta}_{\text{FSA}} &= \left(\bar{\Delta}_{\text{RS}} + \frac{1-K}{2}\right) - \left(\bar{\Delta}_{\text{SA}} + \frac{K^2-1}{12K} \times \frac{a\eta}{a+\eta\theta^\delta C(\delta)} + \frac{1-K}{2}\right) \\ &= (\bar{\Delta}_{\text{RS}} - \bar{\Delta}_{\text{SA}}) - \frac{K^2-1}{12K} \times \frac{a\eta}{a+\eta\theta^\delta C(\delta)} \leq 0. \end{aligned} \quad (27)$$

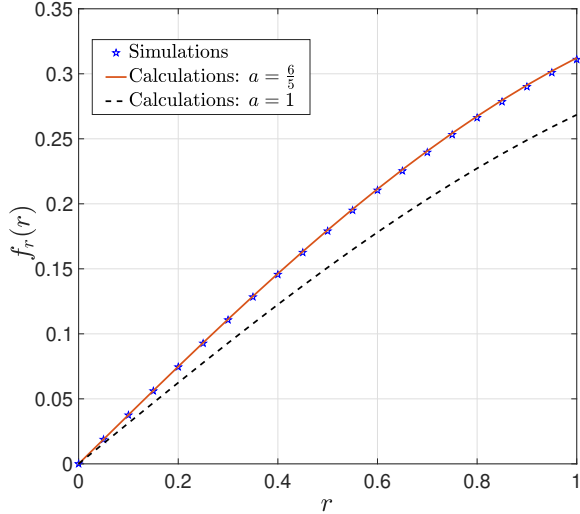


Fig. 3. Pdf of the link distance: simulation results verse calculation results with different rescaled parameters  $a = \frac{6}{5}$  and  $a = 1$ .

In summary, for the special case where  $\theta \rightarrow 0$ , the network average AoI under different channel access schemes follows

$$\bar{\Delta}_{RR} < \bar{\Delta}_{FSA} < \bar{\Delta}_{RS} < \bar{\Delta}_{SA}, \quad (28)$$

which provides an counterintuitive result that the unscheduled FSA introduces implicit regularization over time, enabling it to even outperform the RS strategy.

Given that direct comparisons are challenging, in the following section, we employ numerical results to further illustrate how to select channel access strategies in various scenarios.

#### IV. NUMERICAL RESULTS

In this section, we conduct simulations to examine the effects of different channel access schemes on AoI performance under a range of parameter configurations. Specifically, we model the positions of the DFCs using a Poisson point process with a density of  $\lambda = 5 \times 10^{-2}$  in an area of  $\frac{1600}{\lambda}$  square units. This approach allows the spatial dimensions to adapt according to the density of the DFCs while maintaining an average of 1600 DFCs within the network. The simulation is conducted over  $1 \times 10^5$  time slots, during which we collect and average statistics on AoI. Unless otherwise stated, we set the path loss exponent  $\alpha = 3.8$ , the active probability  $\eta = 0.3$ , and the number of sensors in each cell  $K = 10$ . We determine the revised Rayleigh distribution term  $a = \frac{6}{5}$  through simulation based on these parameters. The error associated with  $a = 1$  without considering network load [18], [19] is illustrated in Fig. 3, contrasting with our findings.

In Fig. 4, we present the network average AoI as a function of the SIR decoding threshold  $\theta$  for the considered channel access schemes. This figure illustrates a close alignment between simulations and theoretical analysis, validating our derivations.

Although the network average AoI deteriorates as  $\theta$  increases (due to the decreased transmission success proba-

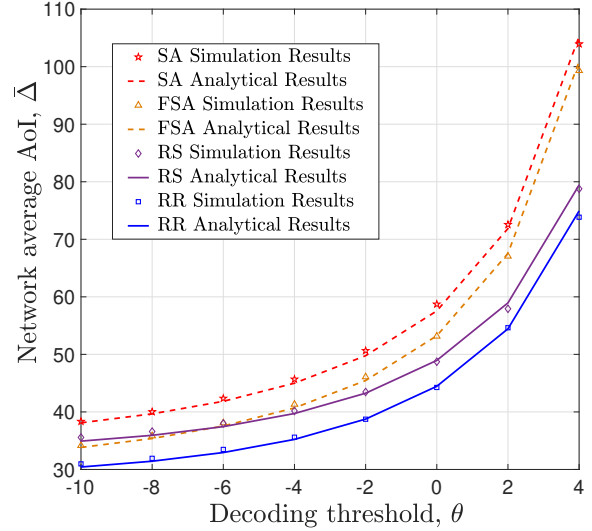
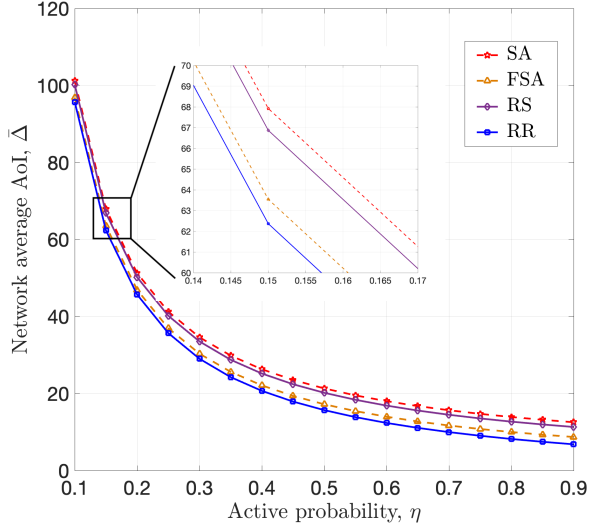


Fig. 4. Network average AoI verse decoding threshold  $\theta$ : simulation results compared to analytical results under different schemes.

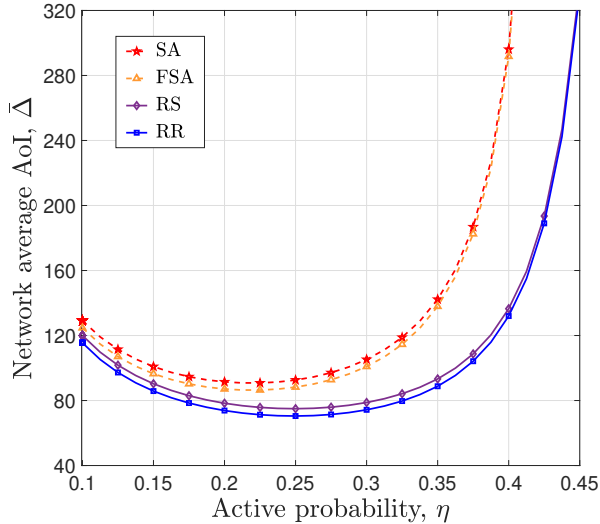
bility associated with higher decoding difficulty), the extent of performance degradation varies notably among the different channel access schemes. Specifically, scheduled schemes demonstrate greater resilience to performance degradation than random access approaches. This resilience is attributed to the scheduled schemes' capacity to coordinate sensors, effectively mitigating intra-cell interference, which improves the SIR and, consequently, the transmission success probability.

The performance gain associated with different channel access schemes also depends on the  $\theta$  values. For instance, at lower  $\theta$  values, the randomized scheduling strategy RS, does not outperform the more structured random access scheme FSA. At lower  $\theta$ , the transmission success probability is already high, so further interference reduction has minimal impact on transmission success probability and does not significantly enhance AoI performance. In this case, a more regularized transmission approach fundamentally improves the network average AoI metric. However, at higher  $\theta$  values, scheduling strategies exhibit a distinct advantage over random access methods.

Fig. 5 plots the network average AoI as a function of the active probability  $\eta$  in two different regimes of  $\theta$  (i.e., the value is very low and relatively high), further illustrating the value of scheduling under varying  $\theta$  conditions. From Fig. 5(a), we observe that the network average AoI decreases monotonically with  $\eta$  in short-packet communication scenarios. In this case, the transmission success probability is close to one, and more frequent updates can enhance information freshness across the network. Moreover, we also validate the performance comparison relationships discussed in III-D. However, the performance differences are relatively minor, suggesting that when performance requirements are not stringent, cost-effective and simple channel access strategies may be viable, as indicated by our analysis.



(a)



(b)

Fig. 5. Network average AoI versus active probability  $\eta$  under different channel access strategies: (a) small decoding threshold in which we set  $\theta = -20\text{dB}$  and (b) large decoding threshold in which we set  $\theta = 4\text{dB}$ .

On the other hand, Fig. 5(b) reveals distinct behavior in long-packet communication scenarios: an optimal active probability exists that minimizes AoI, due to the trade-off between information timeliness and interference levels across the network. Besides, in this context, implementing scheduled channel access schemes evidently shows an advantage in enhancing AoI, with the ranking of schemes as follows

$$\bar{\Delta}_{\text{RR}} < \bar{\Delta}_{\text{RS}} < \bar{\Delta}_{\text{FSA}} < \bar{\Delta}_{\text{SA}}. \quad (29)$$

## V. CONCLUSION

In this paper, we present a comprehensive analysis of the effect of channel access schemes on network AoI performance.

We developed an analytical framework incorporating key system factors, including spatial topology, update rates, interference, and channel access schemes. Based on this model, we derived analytical expressions for the network average AoI under four protocols: SA, FSA, RS, and RR. Our findings highlight that the effectiveness of scheduled access schemes in enhancing AoI performance is closely tied to the SIR decoding threshold. When the threshold is low, the additional scheduling costs may not yield substantial performance benefits. Conversely, as the threshold increases, the advantages of scheduled access become more pronounced, particularly as competition among transmitters intensifies with higher update rates. This study provides valuable insights for practical system design.

## APPENDIX

### A. Proof of Lemma 1

By substituting (5) into (6), we have

$$\begin{aligned} \mu_{0,\text{R}}^{\Phi} &= \mathbb{P} \left( \frac{P_{\text{tx}} h_0 r^{-\alpha}}{\sum_{x_i \in \Phi_{\text{f}}^{\text{R}}} P_{\text{tx}} h_i v_i \|x_i\|^{-\alpha}} > \theta \middle| \Phi \right) \\ &= \mathbb{E} \left[ \prod_{x_i \in \Phi_{\text{f}}^{\text{R}}} \exp(-\theta r^{\alpha} h_i v_i \|x_i\|^{-\alpha}) \middle| \Phi \right] \\ &\stackrel{(a)}{=} \prod_{x_i \in \Phi_{\text{f}}^{\text{R}}} \left( \frac{\eta/K}{1 + \theta r^{\alpha} \|x_i\|^{-\alpha}} + 1 - \frac{\eta}{K} \right), \end{aligned} \quad (30)$$

where (a) holds because  $h_i$  and  $v_i$  are independent in both space and time. We then arrive at the result by further simplifying the expression.

### B. Proof of Theorem 1

We decondition on the expression (9), resulting in the network average AoI given as  $\bar{\Delta}_{\text{SA}} = \frac{K}{\eta} \mathbb{E} \left[ \frac{1}{\mu_{0,\text{R}}^{\Phi}} \right]$ . With the expression (8), we can derive the  $\mathbb{E} \left[ \frac{1}{\mu_{0,\text{R}}^{\Phi}} \right]$  as follows

$$\begin{aligned} \mathbb{E} \left[ \frac{1}{\mu_{0,\text{R}}^{\Phi}} \right] &= \mathbb{E} \left[ \prod_{i \in \Phi_{\text{f}}^{\text{R}}} \left( 1 + \frac{\eta/K}{1 - \frac{\eta}{K} + \frac{\|x_i\|^{-\alpha}}{\theta r^{\alpha}}} \right) \right] \\ &\stackrel{(a)}{=} \mathbb{E} \left[ \exp \left( K \lambda \int_{x \in \mathbb{R}^2} \frac{\eta/K}{1 - \frac{\eta}{K} + \frac{\|x\|^{-\alpha}}{\theta r^{\alpha}}} dx \right) \right] \\ &\stackrel{(b)}{=} \mathbb{E} \left[ \exp \left( 2\lambda\pi \int_0^{\infty} \frac{\eta}{1 - \frac{\eta}{K} + \frac{v^{\alpha}}{\theta r^{\alpha}}} v dv \right) \right] \\ &= \int_0^{\infty} 2a\lambda\pi r \exp \left( -a\lambda\pi r^2 + \int_0^{\infty} \frac{2\lambda\pi\eta}{1 - \frac{\eta}{K} + \frac{v^{\alpha}}{\theta r^{\alpha}}} v dv \right) dr \\ &\stackrel{(c)}{=} \int_0^{\infty} a \exp \left( -az + z\eta\delta \int_0^{\infty} \frac{u^{\delta-1} du}{1 - \frac{\eta}{K} + \frac{u}{\theta}} dz \right) dz \\ &\stackrel{(d)}{=} \int_0^{\infty} a \exp \left( -az + z\eta \left( 1 - \frac{\eta}{K} \right)^{\delta-1} \theta^{\delta} \frac{\pi\delta}{\sin(\pi\delta)} \right) dz, \end{aligned} \quad (31)$$

where (a) stems from the the probability generating functional (PGFL) of PPP [18], (b) involves changing variables from rectangular to polar coordinates, (c) conducts some variable substitutions, including  $z = \lambda\pi r^2$ ,  $v = rq^{\frac{1}{\alpha}}$ , and  $u = q^{\frac{1}{\delta}}$ , and (d) results from the outcome  $\int_0^{\infty} \frac{u^{\delta-1} du}{u+m} = m^{\delta-1} \frac{\pi}{\sin(\pi\delta)}$  [15].

Set  $g_{(\theta,\delta)}(\eta, K) = \eta(1 - \frac{\eta}{K})^{\delta-1} \theta^\delta \frac{\pi^\delta}{\sin(\pi\delta)}$ , we know that if  $g_{(\theta,\delta)}(\eta, K) - a < 0$ ,

$$\int_0^\infty \exp\left(\left(-a + g_{(\theta,\delta)}(\eta, K)\right)z\right) dz = -\frac{1}{g_{(\theta,\delta)}(\eta, K) - a}; \quad (32)$$

otherwise,  $\int_0^\infty \exp\left(\left(-a + g_{(\theta,\delta)}(\eta, K)\right)z\right) dz \rightarrow \infty$ .

With these pieces and the identity  $\frac{\pi^\delta}{\sin(\pi\delta)} = \Gamma(1-\delta)\Gamma(1+\delta)$ , we can get the result outlined in the theorem.

### C. Proof of Theorem 3

Similar to the proof of Theorem 1, we can calculate the mean of  $\frac{1}{\mu_{0,S}^\Phi}$  as follows

$$\begin{aligned} \mathbb{E}\left[\frac{1}{\mu_{0,S}^\Phi}\right] &= \mathbb{E}\left[\prod_{i \in \Phi_S^\dagger} \left(1 + \frac{\eta}{1 - \eta + \frac{D_i^\alpha}{\theta r^\alpha}}\right)\right] \\ &\stackrel{(a)}{=} \mathbb{E}\left[\exp\left(-\int_{x \in \mathbb{R}^2} \frac{\eta}{1 - \eta + \frac{D_i^\alpha}{\theta r^\alpha}} \lambda(x) dx\right)\right] \\ &= \mathbb{E}\left[\exp\left(2\pi \int_0^\infty \frac{\eta \lambda (1 - e^{-\frac{12}{5} \lambda \pi v^2})}{1 - \eta + \frac{v^\alpha}{\theta r^\alpha}} v dv\right)\right] \\ &= \int_0^\infty 2a \lambda \pi r \exp\left(-a \lambda \pi r^2 + \int_0^\infty \frac{2 \lambda \pi \eta (1 - e^{-\frac{12}{5} \lambda \pi v^2})}{1 - \eta + \frac{v^\alpha}{\theta r^\alpha}} v dv\right) dr \\ &= \int_0^\infty a \exp\left(-az + z \int_0^\infty \frac{\eta (1 - e^{-\frac{12}{5} z q})}{1 - \eta + \frac{q^{1/\delta}}{\theta}} dq\right) dz, \quad (33) \end{aligned}$$

where (a) follows from the PGFL of inhomogeneous PPP and the intensity function is according to Approximation 1. With this result, we can decondition  $\mu_{0,S}^\Phi$  in (17), and obtain the conclusion presented in Theorem 3.

### D. Proof of Lemma 3

Drawing parallels with the graphical method delineated in [10], we describe  $n$  the total number of updates received. Depicted in Fig. 2, we calculate the average AoI by summing the AoI of each received update (i.e.,  $A_w$ ), and then dividing by the total time from the start to the receipt of each update (i.e.,  $I_w$ ). As defined in (2), when  $n$  goes to infinity, this formula represents the time-average AoI

$$\bar{\Delta}_0 = \lim_{n \rightarrow \infty} \frac{\sum_{w=1}^n A_w}{\sum_{w=1}^n I_w} = \frac{\mathbb{E}\left[\sum_{i=1}^I i\right]}{\mathbb{E}[I]} = \frac{1}{2} + \frac{\mathbb{E}[I^2]}{2\mathbb{E}[I]}. \quad (34)$$

Under round robin protocol, each sensor is afforded an opportunity to transmit updates at every  $K$  slot. We establish  $X$  as the count of rounds that elapse between two consecutive successful updates, notably obeys a geometric distribution with parameter  $\eta\mu_0^\Phi$ , therefore,  $\mathbb{E}[X] = \frac{1}{\eta\mu_0^\Phi}$  and  $\mathbb{E}[X^2] = \frac{2 - \eta\mu_0^\Phi}{(\eta\mu_0^\Phi)^2}$ . By denoting  $I_w = KX_w$ , we can get the following

$$\mathbb{E}[I] = K\mathbb{E}[X], \quad (35)$$

$$\mathbb{E}[I^2] = K^2\mathbb{E}[X^2]. \quad (36)$$

Combining the above results, the expression of the average AoI under round robin is given by

$$\bar{\Delta}_{0,RR}^\Phi = \frac{1}{2} + \frac{K^2\mathbb{E}[X^2]}{2K\mathbb{E}[X]} = \frac{1}{2} + \frac{K^2 \frac{2 - \eta\mu_0^\Phi}{(\eta\mu_0^\Phi)^2}}{2K \frac{1}{\eta\mu_0^\Phi}}. \quad (37)$$

Subsequent to further simplification, we arrive at the result outlined in Lemma 3.

### REFERENCES

- [1] N. Pappas, M. Abd-Elmagid, B. Zhou, W. Saad, and H. Dhillon, *Age of Information: Foundations and Applications*. Cambridge University Press, 2023.
- [2] S. Kaul, R. Yates, and M. Gruteser, "Real-time status: How often should one update?" in *Proc. IEEE INFOCOM, Orlando, FL, USA*, Mar. 2012, pp. 2731–2735.
- [3] R. D. Yates and S. K. Kaul, "The age of information: Real-time status updating by multiple sources," *IEEE Trans. Inf. Theory*, vol. 65, no. 3, pp. 1807–1827, Mar. 2019.
- [4] —, "Status updates over unreliable multiaccess channels," in *Proc. IEEE Int. Symp. Inf. Theory (ISIT), Aachen, Germany*, Aug. 2017, pp. 331–335.
- [5] X. Chen, K. Gatsis, H. Hassani, and S. S. Bidokhti, "Age of information in random access channels," *IEEE Trans. Inf. Theory*, vol. 68, no. 10, pp. 6548–6568, Oct. 2022.
- [6] J. Sun, Z. Jiang, B. Krishnamachari, S. Zhou, and Z. Niu, "Closed-form whittle's index-enabled random access for timely status update," *IEEE Trans. Commun.*, vol. 68, no. 3, pp. 1538–1551, Mar. 2020.
- [7] H. H. Yang, A. Arafa, T. Q. S. Quek, and H. V. Poor, "Optimizing information freshness in wireless networks: A stochastic geometry approach," *IEEE Trans. Mobile Comput.*, vol. 20, no. 6, pp. 2269–2280, Jun. 2021.
- [8] H. H. Yang, M. Song, C. Xu, X. Wang, and T. Q. Quek, "Locally adaptive status updating for optimizing age of information in Poisson networks," *IEEE Trans. Mobile Comput.*, vol. 22, no. 12, pp. 7343–7354, Dec. 2022.
- [9] F. Zhao, N. Pappas, C. Ma, X. Sun, T. Q. Quek, and H. H. Yang, "Age-threshold slotted ALOHA for optimizing information freshness in mobile networks," *IEEE Trans. Wireless Commun.*, vol. 23, no. 11, pp. 17 236–17 251, Nov. 2024.
- [10] Z. Yue, H. H. Yang, M. Zhang, and N. Pappas, "Age of information under frame slotted ALOHA-based status updating protocol," *IEEE J. Sel. Areas Commun.*, vol. 41, no. 7, pp. 2071–2089, July. 2023.
- [11] I. Kadota, A. Sinha, E. Uysal-Biyikoglu, R. Singh, and E. Modiano, "Scheduling policies for minimizing age of information in broadcast wireless networks," *IEEE/ACM Trans. Netw.*, vol. 26, no. 6, pp. 2637–2650, Dec. 2018.
- [12] M. Haenggi, *Stochastic Geometry for Wireless Networks*. Cambridge University Press, Cambridge, 2012.
- [13] H. H. Yang, C. Xu, X. Wang, D. Feng, and T. Q. S. Quek, "Understanding age of information in large-scale wireless networks," *IEEE Trans. Wireless Commun.*, vol. 20, no. 5, pp. 3196–3210, May 2021.
- [14] F. Baccelli and B. Błaszczyszyn, *Stochastic Geometry and Wireless Networks. Volume I: Theory*. Now Publishers, 2009.
- [15] M. Haenggi, "The meta distribution of the SIR in Poisson bipolar and cellular networks," *IEEE Trans. Wireless Commun.*, vol. 15, no. 4, pp. 2577–2589, Apr. 2016.
- [16] —, "User point processes in cellular networks," *IEEE Wireless Commun. Lett.*, vol. 6, no. 2, pp. 258–261, Apr. 2017.
- [17] T. D. Novlan, H. S. Dhillon, and J. G. Andrews, "Analytical modeling of uplink cellular networks," *IEEE Trans. Wireless Commun.*, vol. 12, no. 6, pp. 2669–2679, Jun. 2013.
- [18] J. G. Andrews, A. K. Gupta, and H. S. Dhillon, "A primer on cellular network analysis using stochastic geometry," *arXiv preprint arXiv:1604.03183*, Apr. 2016.
- [19] H. ElSawy and E. Hossain, "On stochastic geometry modeling of cellular uplink transmission with truncated channel inversion power control," *IEEE Trans. Wireless Commun.*, vol. 13, no. 8, pp. 4454–4469, Aug. 2014.